ISPRS Journal of Photogrammetry and Remote Sensing 152 (2019) 1–12

Contents lists available at ScienceDirect

ISPRS Journal of Photogrammetry and Remote Sensing

journal homepage: www.elsevier.com/locate/isprsjprs

Spatial, temporal, and spectral variations in albedo due to vegetation changes in China's grasslands

Lei Zheng[a,b,1], Guosong Zhao[a,1], Jinwei Dong[a,b,*], Quansheng Ge[a], Jian Tao[c], Xuezhen Zhang[a], Youcun Qi[d], Russell B. Doughty[e], Xiangming Xiao[e,f]

[a] Key Laboratory of Land Surface Pattern and Simulation, Institute of Geographic Sciences and Natural Resources Research, Chinese Academy of Sciences, Beijing 100101, China
[b] University of Chinese Academy of Sciences, Beijing 100049, China
[c] College of Public Administration, Shandong Technology and Business University, Yantai 264005, China
[d] Key Laboratory of Water Cycle and Related Land Surface Processes, Institute of Geographic Sciences and Natural Resources Research, Chinese Academy of Sciences, Beijing 100101, China
[e] Department of Microbiology and Plant Biology, and Center for Spatial Analysis, University of Oklahoma, Norman, OK 73019, USA
[f] Ministry of Education Key Laboratory of Biodiversity Science and Ecological Engineering, Institute of Biodiversity Science, Fudan University, Shanghai 200438, China

ARTICLE INFO

Keywords:
Albedo
Greenness
Grassland
Climate change
China

ABSTRACT

Changes in Earth's albedo due to vegetation dynamics, snow cover, and land cover change have attracted much attention. However, the effects of vegetation dynamics on albedo have not been comprehensively documented according to its spatial (regional), temporal (within growing season), and spectral (visible, near-infrared, and shortwave) characteristics. This study examined the effects of vegetation greenness on albedo from 2000 to 2014 in China's grasslands, which have considerable intra- and inter-annual variations, using remote sensing-based albedo and two-band Enhanced Vegetation Index (EVI2) data. Generally, we found an insignificant negative correlation between the shortwave (SW) albedo and EVI2 for grasslands in China. However, the visible (VIS) albedo was more sensitive to changes in vegetation greenness than near-infrared (NIR) albedo in China's grasslands. The relationship between the NIR albedo and EVI2 was more complicated, especially in the Tibetan Plateau (TP), where the correlation was negative in the early growing season and positive in the late growing season; while the correlation between the NIR albedo and EVI2 was always negative in main part of Inner Mongolia (IM). The different albedo-EVI2 relationships in IM and TP may be related to differences in soil albedos. The higher sensitivity of the SW albedo to vegetation greenness change in IM, the stronger effect on land surface radiation budget. Our finding about vegetation-induced changes in albedo differ in space, time and spectral bands is expected to contribute to the improvement of land surface models.

1. Introduction

Land surface albedo, defined as the ratio of the total radiation reflected from a surface to the total incoming radiation that falls on it, is a fundamental variable in the land surface radiation budget (Moody et al., 2007). Land surface albedo is affected by numerous interrelated factors including snow, vegetation, soil moisture, and solar zenith angle (He et al., 2014; Li et al., 2018; Loarie et al., 2011). The contribution of snow cover to land surface albedo is large due to its high reflectance (Moody et al., 2007). However, the effect of changes in vegetative cover on land surface albedo also plays a crucial role in the land surface radiation budget. For example, previous simulations found that deforestation increased albedo and cooled down the Northern Hemisphere (Brovkin et al., 2006; Govindasamy et al., 2001), while forestation in temperate and boreal forest areas could decrease surface albedo and offset potential carbon uptake (Betts, 2000).

Earth has been experiencing a greening trend as a result of CO_2 fertilization, nitrogen deposition, climate change, and land cover change (Zhu et al., 2016). The ongoing greening can influence regional and global climate by altering surface albedo, surface roughness, and the hydrologic cycle (Bonan, 2008; Li et al., 2018; Zeng et al., 2017). Therefore, investigating the changes in surface albedo due to vegetation

* Corresponding author at: Institute of Geographic Sciences and Natural Resources Research, Chinese Academy of Sciences, 11A, Datun Road, Chaoyang District, Beijing 100101, China.
E-mail address: dongjw@igsnrr.ac.cn (J. Dong).
[1] These authors contributed equally to this work.

https://doi.org/10.1016/j.isprsjprs.2019.03.020
Received 11 November 2018; Received in revised form 21 March 2019; Accepted 30 March 2019

and land cover dynamics is vital to understanding their role in earth's changing climate. Overall, the land surface albedo in the growing season is a combination of the vegetation and soil albedos. The main factor determining which of the two albedos has the strongest influence on the overall surface albedo is the fractional area covered by each of vegetation and soil (Kala et al., 2014; Rechid et al., 2009; Wang et al., 2016). Vegetation affects albedo in two ways. One way is to change the contribution of soil albedo to overall albedo (Hammerle et al., 2007; Rechid et al., 2009). When vegetation becomes greener with higher leaf area index (LAI), more incoming solar energy is reflected, scattered, and/or absorbed by the vegetation canopy, and only a small proportion of radiation reaches the ground. The other way is the optical and structural properties of the vegetation canopy itself, for example, plant mean stand age, plant height, plant biomass, and vegetation species composition (Lukeš et al., 2014; Kuusinen et al., 2016).

Grassland ecosystems in China play an important role in the global biogeochemical cycle. The temperate grassland in Inner Mongolia (IM) is the third largest in the world (Lee et al., 2002), and the grassland of the Tibetan Plateau (TP) is earth's largest alpine ecosystem (Coners et al., 2016). Thus, it is of great significance to understand how changes in grassland cover in China affect albedo. Grassland ecosystems, dominated by therophytes, show remarkable temporal (i.e. seasonal and inter-annual) and spatial variations that affect surface albedo (Tian et al., 2014; Wang and Davidson, 2007). Previous studies have found a significant negative correlation between changes in grassland and land surface albedo during the growing season in the TP using Normalized Difference Vegetation Index (NDVI) (Shen et al., 2015; Tian et al., 2014). Tian et al. (2017) also found that changes in grassland greenness which indicated by NDVI during the growing season had a greater effect on albedo in the TP than the snow cover during the non-growing season.

Albedo is variable in different spectrum bands and across different land cover types. Earth's albedo is the amount of the diffuse reflection of solar radiation, which is shortwave (SW) electromagnetic radiation generally in the range of 0.3–5.0 μm. Within this SW spectrum, the visible (VIS, 0.3–0.7 μm) and near-infrared (NIR, 0.7–5.0 μm) broadbands are frequently used to detect and monitor vegetation due to its marked difference in reflectance in these two spectral regions compared to non-vegetated land cover (Liang et al., 2003). Correlations between vegetation change and albedo in SW, NIR and VIS broadbands vary with vegetation types and canopy densities (Blok et al., 2011; Hammerle et al., 2007; Kuusinen et al., 2016; Lukeš et al., 2016). For example, the deciduous broadleaf forests show a higher albedo in the NIR and SW broadbands but lower albedo in VIS broadband in summer (Gao et al., 2005).

Correlations between albedo and vegetation dynamics also show temporal variability (Wang and Davidson, 2007). However, the seasonal variability of albedo due to changes in vegetation during the growing season is not explicitly understood. For example, changes in carbon and water fluxes due to climate change in the temperate grasslands of Inner Mongolia contrast the fluxes in the alpine grasslands of the Tibetan Plateau (Liu et al., 2018), and the different responses by vegetation to climate change could affect seasonal and inter-annual albedo differently in the two regions. Specifically, Liu et al. (2018) found that soil moisture is the major limiting factor in IM while grasslands in TP are much more limited by thermal conditions. Further, it is unclear whether the relationships of albedo and grassland ecosystem dynamics are the same in two different grassland types (IM and TP). First, little is known about whether the negative relationships between albedo and vegetation greening in the two regions are consistent in each month of growing season. Second, it is not known if there are differences between the VIS and NIR parts of the albedo spectrum.

In this study, we used remotely sensed albedo and 2-band Enhanced Vegetation Index (EVI2) data which was designed for sensors with no blue band and corresponded well with the original EVI (Jiang et al., 2008) to examine the characteristics of the relationship between albedo and grassland greenness from three aspects: (1) the VIS and NIR parts of the albedo spectrum; (2) different months among growing season; and (3) different geographic regions or grassland types. More specifically, we addressed the following questions: (1) Did VIS or NIR albedo correlate with grassland greenness, and which part of the albedo spectrum was more sensitive to changes in greenness? (2) How did the relationship between albedo and grassland greenness vary between different months of the growing season? (3) Was this temporal variability consistent in different grasslands (e.g., temperate grassland in IM and alpine grassland in TP)? The answers to these questions would contribute to our understanding of the variability and drivers of the land surface energy budget in the context of climate change.

2. Data and methods

2.1. Study area

The study area includes all grasslands of China, which encompasses 13 provinces. While the sparse grasslands in Xinjiang were included in this study, we generally focused on the temperate and alpine grasslands in Inner Mongolia and Tibetan Plateau. The temperate grassland is generally located in the northeastern part of China, mainly Inner Mongolia (IM), where it is strongly influenced by the temperate monsoon climate. Its annual precipitation is above 450 mm with the rainy season in summer (June-August), while the mean annual temperature ranges from −3 °C to 9 °C across the temperate grassland (Zhang et al., 2014). Annual precipitation decreases from the meadow steppe of the east to the desert steppe of the west (Kang et al., 2007). The southwest part of the study area is in the Tibetan Plateau (TP), which is strongly influenced by the alpine climate. The mean annual temperature ranges from −15 °C to 5 °C (You et al., 2013). Annual precipitation in the plateau grassland shows a southeastward increasing pattern ranging from 100 to 700 mm, and the primary grassland types include alpine steppe and alpine meadow (Yang et al., 2010b).

2.2. Data

2.2.1. Grassland cover data

The grassland extent was defined by using the Moderate Resolution Imaging Spectroradiometer (MODIS) annual land cover type products (MCD12C1.005) at a 0.05° spatial resolution with the International Geosphere-Biosphere Program (IGBP) land cover scheme (Friedl et al., 2010). To avoid the disturbance from land cover changes, we defined grassland pixels as those pixels that were classified as grassland > 90% of the time between 2001 and 2012.

2.2.2. Vegetation greenness data

Vegetation greenness was obtained from the Vegetation Index and Phenology (VIP) Vegetation Indices Monthly Global datasets (version 4), which was developed by the VIP Research Lab at the University of Arizona, with a spatial resolution of 0.05° (Didan and Barreto, 2016). This version was improved by a two-step filtering approach of the input data and using a new per pixel continuity algorithm at a monthly step, which improved the data quality and spatial consistency compared to version 3. We used the gap-filled monthly 2-band Enhanced Vegetation Index (EVI2) from the VIP30 product (Jiang et al., 2008) as a proxy of vegetation greenness, which was generated based on the MODIS surface reflectance data (MOD09) from 2000 to 2014. The VIP EVI2 product has been used in the Mongolian Plateau (Chen et al., 2015), the Northern Hemisphere (Kim et al., 2014), and the global scale (Zhang et al., 2015), all showing the reliability of this dataset.

2.2.3. Albedo data

The albedo data was obtained from the Global Land Surface Satellite (GLASS) remote sensing products, which were produced and distributed by the Center for Global Change Data Processing and Analysis at Beijing

Normal University (http://www.geodata.cn). The GLASS albedo products have a similar accuracy to that of the MODIS MCD43 albedo products according to a homogeneous FLUXNET sites-based validation (53 sites) and multi-products cross-validation, and have improved data gap-filling and smoothing algorithms to generate gapless and continuous datasets (He et al., 2014; Liu et al., 2013; Ma et al., 2017). We used the white sky albedo (WSA) GLASS products (GLASS02B06 V4, 2000/001-2014/361) in this study, which has a spatial resolution of 0.05° and a temporal resolution of 8 days. The 8-day albedo data was aggregated to monthly albedo data using the median value which is an effective solution to the extreme value problem within a month to match the monthly EVI2 data.

2.2.4. Snow cover data

The snow cover dataset (MOD10CM.006) from 2000 to 2014 was obtained from the National Snow and Ice Data Center. The dataset is with a spatial resolution of 0.05° and a monthly temporal resolution, and with the unit of percent per pixel. Depending on the study area, season and validation method, the accuracy of MODIS snow cover products was between 85 and 95%, and snow cover accuracies are generally higher for grassland than that of forest (Coll and Li, 2018).

2.2.5. Energy budget data

The Clouds and Earth's Radiant Energy Systems (CERES) Energy Balanced and Filled (EBAF) edition 4.0 (CERES EBAF-Surface_Ed4.0) was used in this study (Kato et al., 2013), which provided monthly and climatological averages of computed fluxes of Earth's surface. The standard CERES data products used cloud and aerosol properties derived from MODIS radiances, meteorological assimilation data from the Goddard Earth Observing System (GEOS) Version 5.4.1 model, and aerosol assimilation from the Model for Atmospheric Transport and Chemistry. We used surface downward shortwave in this study, which has a spatial resolution of 1°. These data were obtained from the NASA Langley Research Center CERES ordering tool (http://ceres.larc.nasa.gov/).

2.3. Methods

2.3.1. Trend analysis of EVI2 and albedo

The trends of EVI2 and albedo were calculated using the linear regression at two scales: regional scale and pixel scale. The regional scale analysis provided a general picture of trends of vegetation greenness and albedo for the temperate and alpine grasslands as well as the entire study area from 2000 to 2014, while the pixel scale analyses showed the spatial patterns of the EVI2 and albedo. Albedo/EVI2 in a regional scale was done firstly by averaged from the all the pixels in the region in a certain year, then the regional trend of Albedo/EVI2 and relationship between albedo and EVI2 were calculated (Hou et al., 2018). At temporal scales, analyses were conducted for both the growing season, defined as May through September (Shen et al., 2015; Tian et al., 2014), and each month in the growing season. The trend was calculated as the slope of linear regression with the ordinary least squares method:

$$Slope = \frac{n \times \sum_{i=1}^{n} (i \times A_i) - \sum_{i=1}^{n} i \times \sum_{i=1}^{n} A_i}{n \times \sum_{i=1}^{n} i^2 - (\sum_{i=1}^{n} i)^2} \quad (1)$$

where n was the length of the time series that was studied ($n = 15$), i was the number of year, and A_i was albedo or EVI2 in the ith year. We calculated the regression slope and the p-value for each pixel from the EVI2 or albedo time series images. Next, we created maps of increasing or decreasing trends in EVI2 or albedo by using the positive or negative slopes.

2.3.2. Correlation analysis of EVI2 and albedo

To investigate the impacts of vegetation greenness on albedo, we calculated the Pearson's correlation coefficient (r) for EVI2 and albedo (SW, NIR, and VIS) for the entire growing season and also each month of the growing season from 2000 to 2014:

$$r_{xy} = \frac{\sum_{i=1}^{n} (x_i - \bar{x})(y_i - \bar{y})}{\sqrt{\sum_{i=1}^{n} (x_i - \bar{x})^2 \sum_{i=1}^{n} (y_i - \bar{y})^2}} \quad (2)$$

where x_i and y_i were the values of the ith year, $\bar{x}$ and were the average values of all years. When $r > 0$, the two variables were positively correlated, and when $r < 0$, the two variables were negatively correlated. The correlation analyses were performed for the whole period and each month of growing season. Next, we obtained maps showing the variation of correlation between EVI2 and albedo within the growing season.

2.3.3. Relative importance calculation of snow cover and EVI2 to albedo change

We used a relative importance analysis approach to quantify the relative contributions of vegetation greenness and snow cover to changes of albedo in each grid cell (Huang et al., 2018), expressed as the Pearson correlation in a multiple linear regression ($albedo = b_0 + b_1 \times EVI2 + b_2 \times snow\ \ cover + \varepsilon$). ε represented other factors that might contribute to albedo variation. The analysis was performed using the 'relaimpo' package in R, which was based on variance decomposition for multiple linear regression models. One of the most computer-intensive and commonly used methods named 'LMG' was chosen to differentiate contributions of different correlated regressors in a multiple linear regression (Grömping, 2006). The contribution of EVI2 and snow cover were quantified in each grid cell across the study area, and then the higher contribution to the albedo variation was identified as the dominant driver (Hou et al., 2018; Huang et al., 2018).

3. Results

3.1. Trends of greenness and albedo from 2000 to 2014

Growing season mean EVI2 ($EVI2_{GSM}$) showed an insignificant increase ($R^2 = 0.18$, $p = 0.11$, Fig. 1a) from 0.196 in 2000 to 0.202 in 2014 with an increasing rate of 0.00078 $year^{-1}$ across the whole study area. The growing season mean SW albedo (SWA_{GSM}) decreased significantly over the past 15 years, with an average decrease of 0.00030 $year^{-1}$ ($R^2 = 0.57$, $p < 0.05$, Fig. 1b). The growing season mean NIR albedo ($NIRA_{GSM}$) showed a slight but insignificant decrease ($R^2 = 0.08$, $p = 0.32$, Fig. 1c), whereas the growing season mean VIS albedo ($VISA_{GSM}$) showed a significant decrease ($R^2 = 0.65$, $p < 0.05$, Fig. 1d) with a decrease rate of 0.00041 $year^{-1}$.

The spatial patterns of the change rates in $EVI2_{GSM}$, SWA_{GSM}, $NIRA_{GSM}$ and $VISA_{GSM}$ during 2000–2014 were shown in Fig. 2. Most of the grasslands in China experienced a greening trend (67.0%) with 15.3% of the grasslands being statistically significant ($p < 0.05$ hereafter, red in insets of Fig. 2a). One-third (33.0%) of grasslands underwent a decrease in $EVI2_{GSM}$ and only 2.2% were significant (Fig. 2a). Notably, the EVI2 trends varied in different months of the growing season (Fig. S1). Specifically, in May most of the grasslands (80.0%) experienced an increasing trend, while in July only 56.0% of grasslands experienced an increase (Fig. S1 a1, a3).

For SWA_{GSM} and $NIRA_{GSM}$, 78.0% and 52.6% of grasslands experienced decreases, respectively, and were mainly distributed in IM; and 28.5% and 15.6% of pixels were statistically significant for SWA_{GSM} and $NIRA_{GSM}$, respectively. Meanwhile, 22.0% and 47.4% of grasslands had increasing trends in SWA_{GSM} and $NIRA_{GSM}$, respectively. Of these

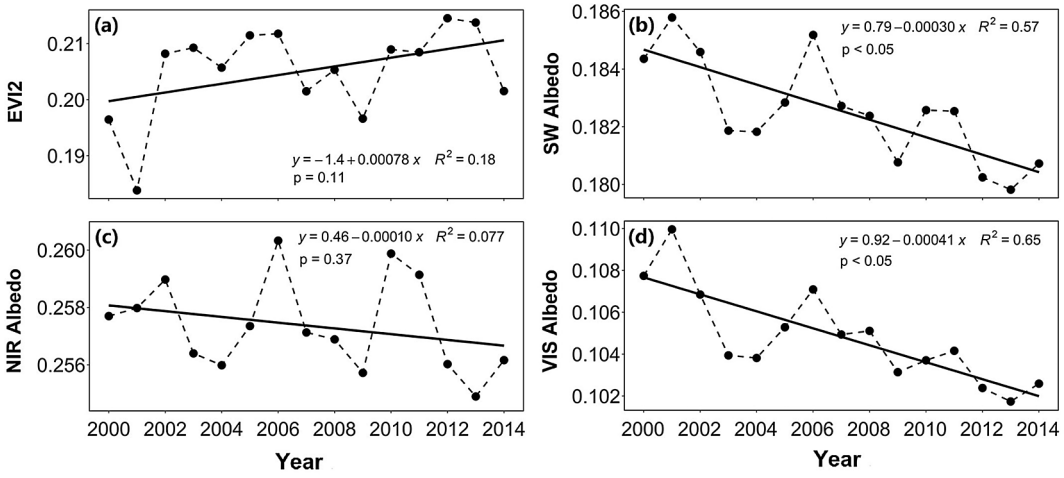

Fig. 1. Inter-annual variations and trends of the growing season mean EVI2 (May–September) (a), SW albedo (b), NIR albedo (c), and VIS albedo (d) over the grasslands in China during the period 2000–2014. Straight lines indicate linear regressions of EVI2, SW albedo, NIR albedo, and VIS albedo against time.

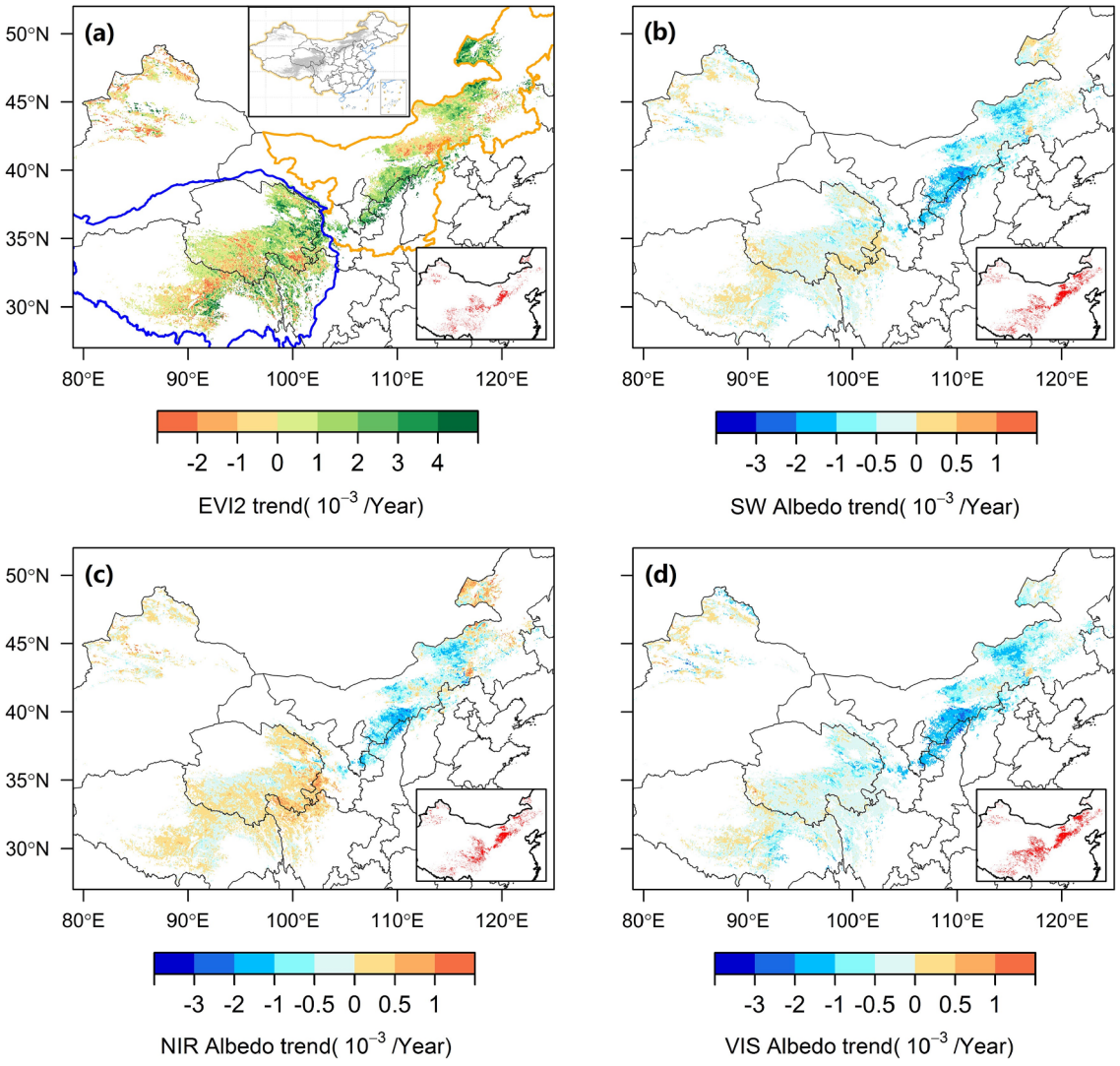

Fig. 2. Spatial pattern of trends in growing season mean EVI2 (a), SW albedo (b), NIR albedo (c), and VIS albedo (d) of grasslands in China. The inset shows the pixels with statistical significance ($p < 0.05$). The top inset in sub-Figure (a) shows the distribution of the studied grassland extent; the blue line in sub-Figure (a) shows the region of the TP; the orange line in sub-Figure (a) shows the region of the IM (Loess Plateau was combined into the IM grassland region given its small proportion of grasslands in this study). (For interpretation of the references to colour in this figure legend, the reader is referred to the web version of this article.)

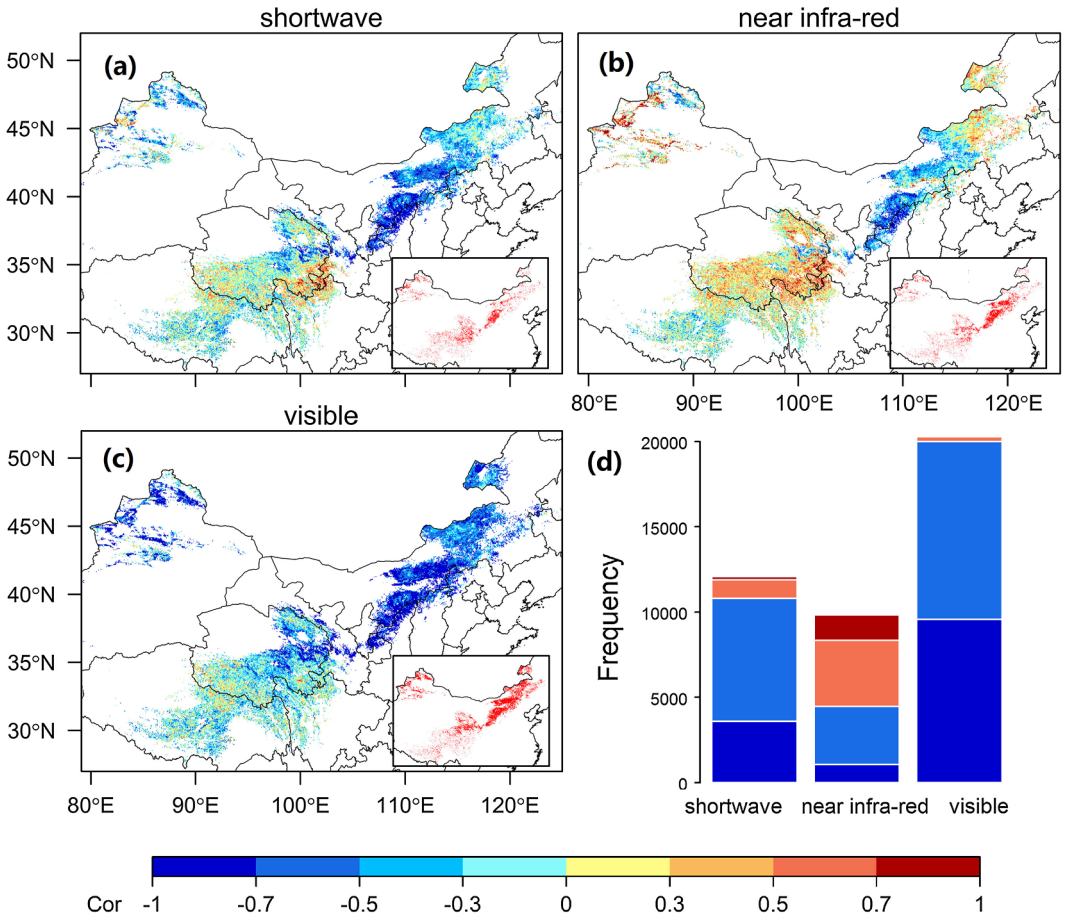

Fig. 3. Correlation coefficients between the growing season mean EVI2 and the SW albedo (a), NIR albedo (b), and VIS albedo (c) in the grasslands of China. The insets indicate the distribution of the pixels that were statistically significant at $p < 0.05$. The bottom right sub-Figure (d) shows the total number of pixels that were significantly correlated with EVI2 for the SW, NIR, and VIS albedos ($p < 0.05$); there were total 55,038 pixels in the studied grasslands.

grasslands, 2.2% and 11.0% had statistically significant increasing trends in SWA_{GSM} and $NIRA_{GSM}$, respectively, and were mainly distributed in the TP and northeast IM (Fig. 2b and c). $VISA_{GSM}$ decreased in most of the study area (87.0%), and the decrease was statistically significant for 35.3% of the pixels (Fig. 2d). The areas with increasing NIR albedo varied from May to September. More than half (54.2%) of the grasslands experienced an increasing trend in NIR albedo during June, which were mainly distributed in the TP and the northeast of IM. However, only 34.7% of grasslands showed an increasing trend in May (Fig. S1 c1, c2).

3.2. Spectral variations in SW, NIR, and VIS albedo changes due to vegetation dynamics

SWA_{GSM} was negatively correlated with $EVI2_{GSM}$ in 68.8% of the grassland pixels with 21.1% of the grassland pixels being statistically significant ($p < 0.05$, hereafter). A positive correlation was found in 31.2% of the pixels with 3.0% being significant (Fig. 3a). For $NIRA_{GSM}$, 56.1% of the grasslands had a positive correlation with 10.8% being significant (Fig. 3b), and 43.9% of the pixels had a negative correlation with 8.2% being significant. The positive correlations were mainly distributed in TP and northeast IM, and the negative correlations were mainly distributed in IM. For $VISA_{GSM}$, negative correlations of albedo and EVI2 were found in most areas (84.8%) with 41.1% being significant (Fig. 3c).

3.3. Monthly variations in SW, NIR, and VIS albedo changes due to vegetation dynamics

The correlation between the SW albedo and EVI2 varied in different months. In each month, the number of negatively correlated grasslands pixels was higher than those with a positive correlation, but the number of pixels with a positive correlation increased from May to September. The proportion of pixels with a positive correlation between SW albedo and EVI2 in each month was 19.3% (May), 23.8% (June), 34.3% (July), 41.7% (August), and 44.3% (September), respectively. Thus, the number of pixels with negative correlations decreased from May to September: 80.7%, 76.2%, 65.7%, 58.3%, and 55.7% respectively. From May to September, the shift from a negative correlation to a positive correlation mainly occurred in TP, while in IM the correlation was consistently negative for most grasslands (Fig. 4a1-a5).

Correlations between the NIR albedo and EVI2 shifted from negative to positive from May to September. The negative correlation between the NIR albedo and EVI2 was obvious in May within 70.6% of study area (Fig. 4b1). By August, the positive correlation became dominant, with 64.3% pixels having a positive correlation (Fig. 4b4). This shift mainly occurred in TP and northeast IM.

The negative correlation between the VIS albedo and EVI2 was stronger than that of the NIR albedo. Most of the grasslands in China showed a negative correlation with significant negative correlation mainly distributed in IM. Grasslands with a negative correlation covered the largest area in June, whose area accounted for 89.2% of the total area. Moreover, the area with a significant negative correlation

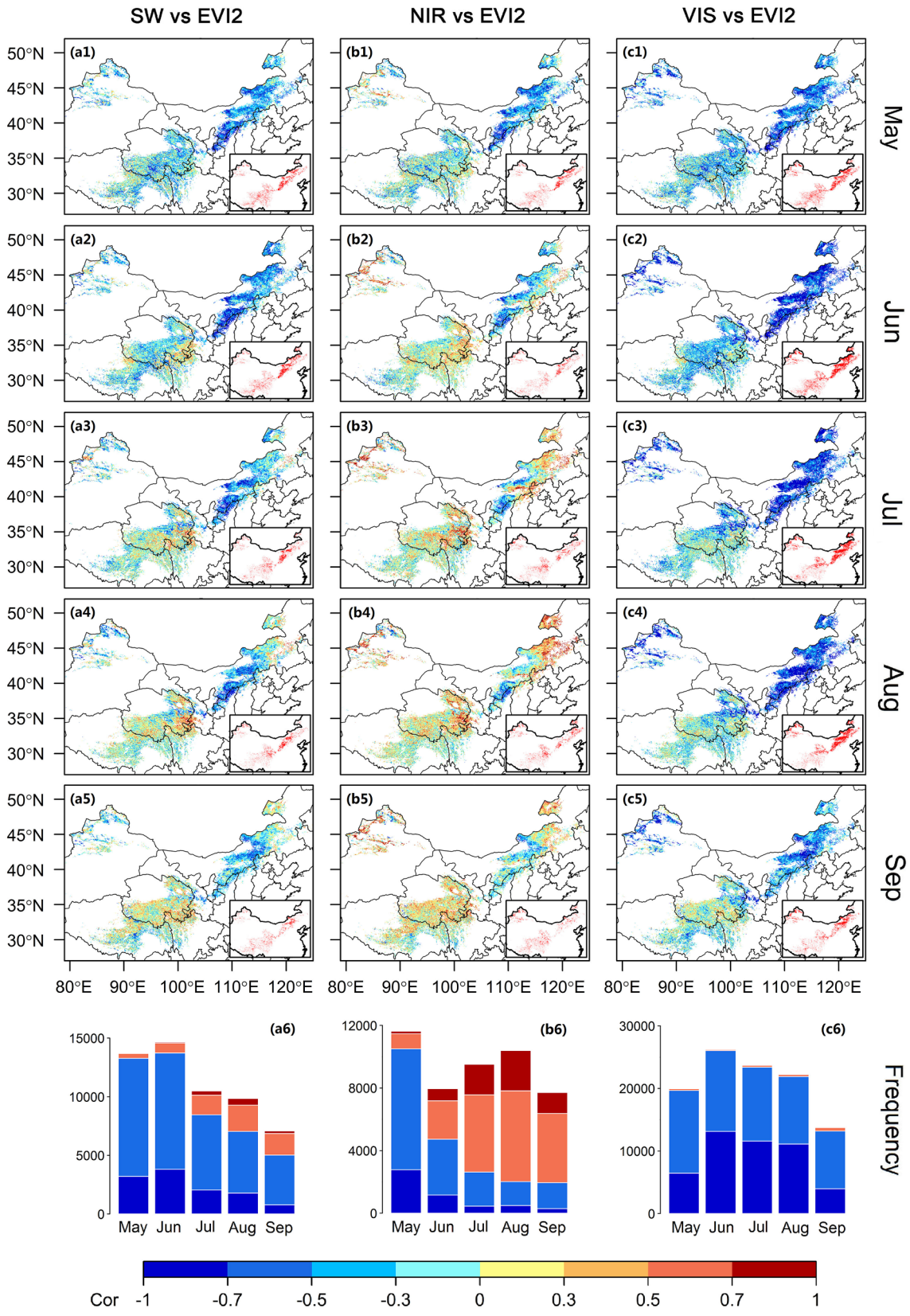

Fig. 4. The spatial pattern of correlation coefficients between EVI2 and SW albedo (a1-a5); NIR albedo (b1-b5); VIS albedo (c1-c5) for grasslands in China from May to September. The insets indicate pixels that were statistically significant at $p < 0.05$. The bottom sub-Figure shows the total number of SW albedo (a6); NIR albedo (b6) and VIS albedo (c6) pixels that were significantly correlated with EVI2 from May to September ($p < 0.05$). There were a total of 55,038 pixels in the studied grasslands.

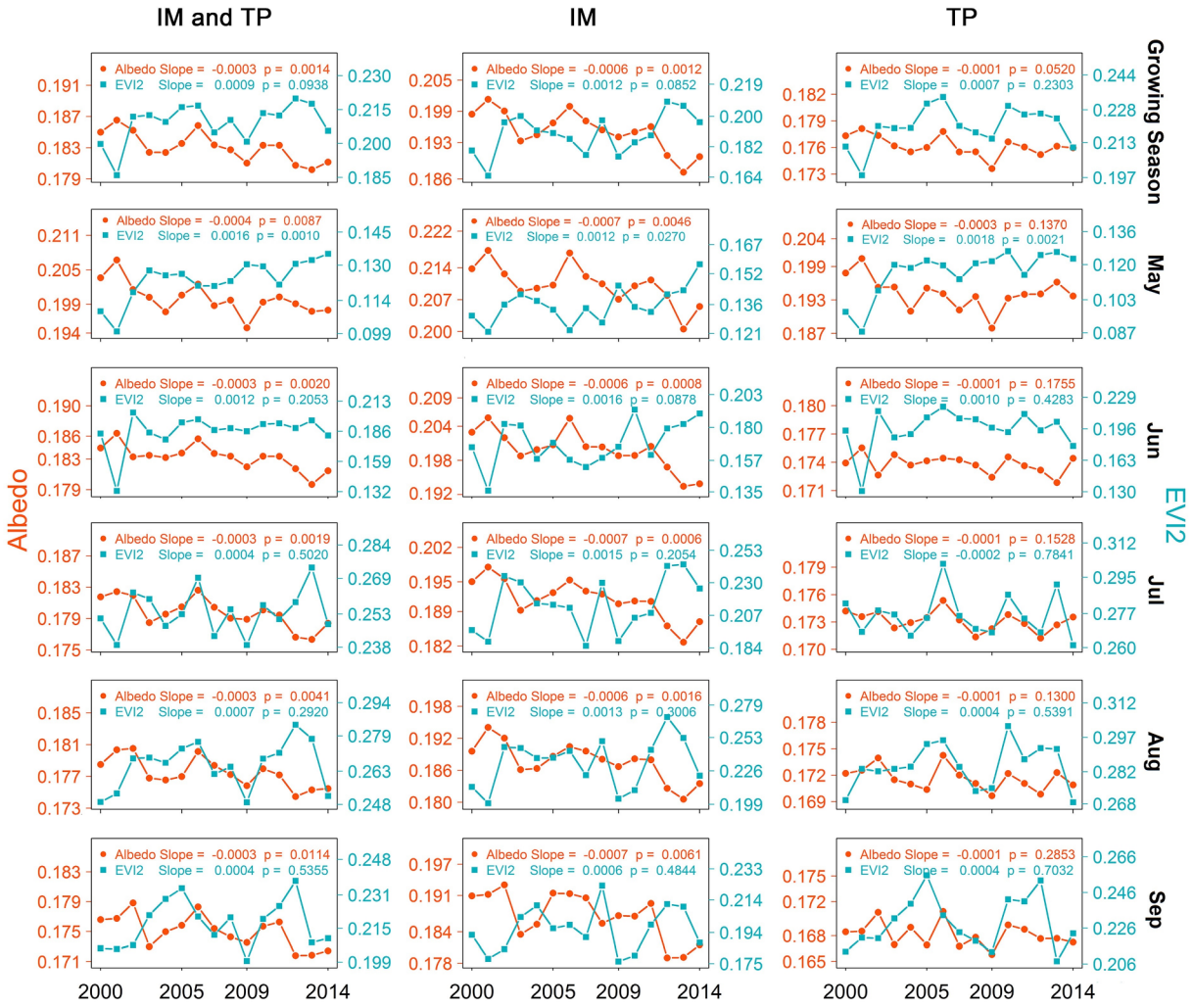

Fig. 5. The inter-annual variability of the monthly SW albedo and monthly EVI2 from 2000 to 2014 in total regions of IM and TP, IM region and TP region.

was notably larger than that of NIR from May to September (Fig. 4c1-c5).

3.4. Spatial variations in SW, NIR, and VIS albedo changes due to vegetation dynamics

The relationship between SW albedo and EVI2 showed spatial heterogeneity. Generally, SW albedo and EVI2 were positively related in TP while they were negatively related in most parts of IM. Therefore, we investigated the changes in albedo in these two regions to examine their spatial patterns (Fig. 2a). It is important to note that we combined the small range of grassland on the edge of the Loess Plateau into the IM zone.

For IM and TP combined, SW albedo significantly decreased during the growing season and each month of the growing season (Fig. 5). However, the significant positive trend ($p < 0.05$) in EVI2 was only found in May. Similarly, for IM (Fig. 5) SW albedo had significant decreasing trends, but a significant increasing trend in EVI2 was only observed in May. For TP, albedo had no significant annual trend for the growing season or growing months (Fig. 5). EVI2 had a significant positive trend only in May. The trends of the monthly NIR and VIS albedo and monthly EVI2 from 2000 to 2014 were shown in Figs. S2 and S3.

The Fig. 6 illustrated the correlations between monthly mean EVI2 and albedo in IM and TP from May to September. For the entire growing season, NIR and EVI2 were negatively correlated in IM and positively correlated in TP. In May, NIR albedo and EVI2 had a significant negative correlation in IM and an insignificant negative correlation in TP. However, from June to September NIR albedo was positively correlated with EVI2 in TP. Meanwhile, the significant negative correlation between NIR albedo and EVI2 in IM was only found in May. The relationship between VIS albedo and EVI2 was insignificant ($p < 0.05$) in TP for July, August, and September. In IM, VIS albedo was significantly negatively correlated with EVI2 for the growing season and each month.

3.5. Potential effects of albedo and vegetation changes on surface net radiation

Overall, the average EVI2 in TP was higher than in IM, and the average albedo in TP was lower than in IM. The regression slope values of EVI2 to SW albedo were −0.23 (growing season), −0.39 (May), −0.15 (June), −0.12 (July), −0.08 (August) and −0.16 (September) in IM and were −0.01, −0.16, −0.02, 0.06, 0.03, and 0.01 in TP.

Based on the linear regressions of albedo and EVI2 as shown in Fig. 6, we further calculated that the response of the surface absorbed downward shortwave radiation to a small change of 0.01 in EVI2 (Fig. 7). The regression slopes of EVI2 and SW albedo in Fig. 6 were multiplied by the regional mean surface downward shortwave of EBAD-Surface product to calculate the monthly variation of the surface absorbed downward shortwave radiation. Positive values represented more energy absorption and negative values represented the opposite.

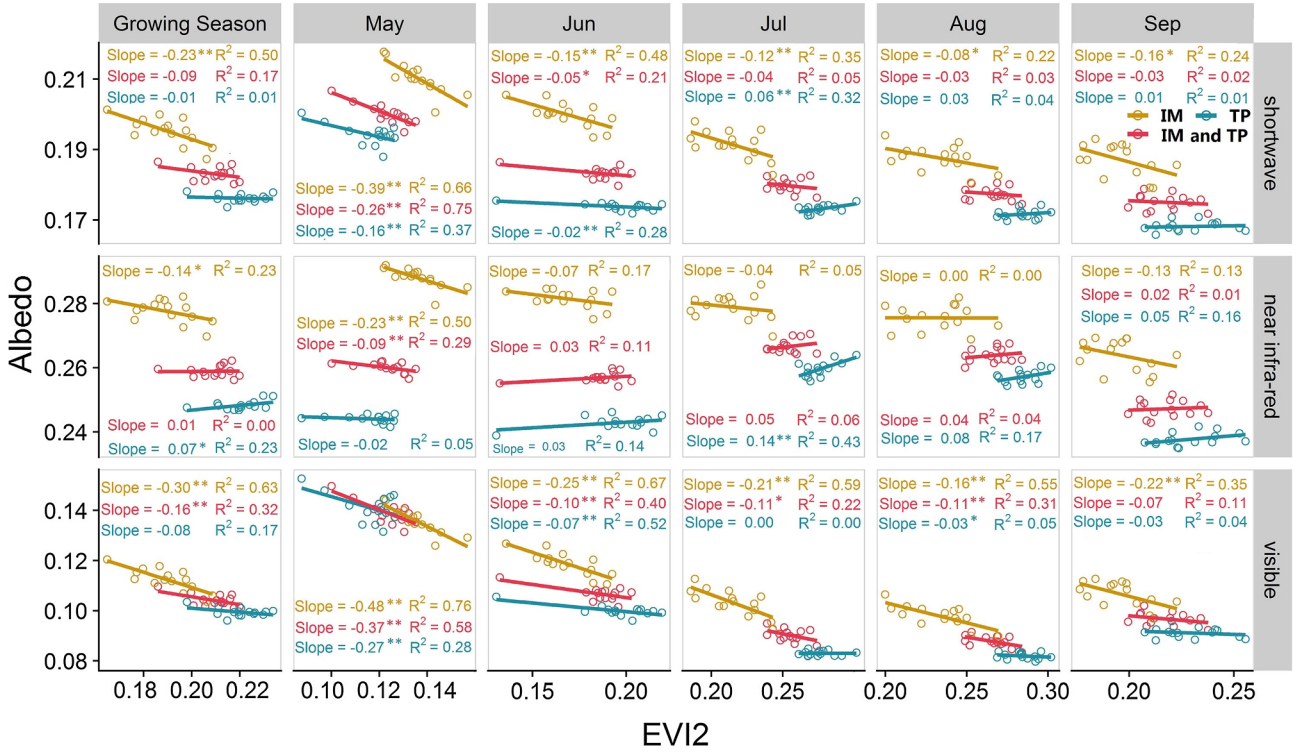

Fig. 6. The correlations between the monthly mean EVI2 and albedo from May to September. The yellow points and regression line correspond to the IM region; the blue points and regression lines correspond to the TP region; the red points and regression lines correspond to the total regions of IM and TP. $^{*}p < 0.1$, $^{**}p < 0.05$. (For interpretation of the references to colour in this figure legend, the reader is referred to the web version of this article.)

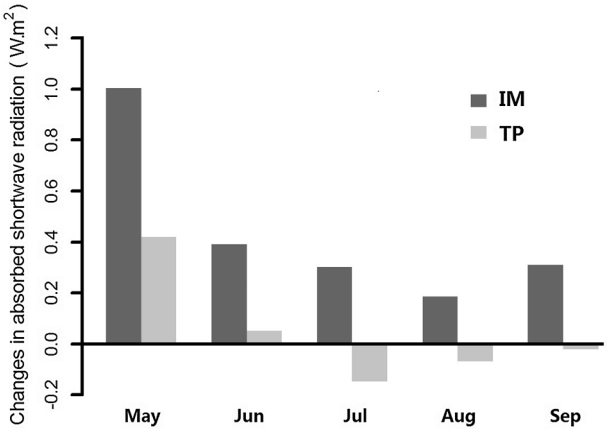

Fig. 7. The variation of the absorbed downward shortwave radiation caused by an increase of EVI2 by 0.01, according to the linear regressions of albedo and EVI2 (Fig. 6).

In May, an increase in EVI2 by 0.01 led to an increase in absorbed downward shortwave radiation, reaching 1.00 Wm^{-2} in IM. In June, July, August, and September, the corresponding values were 0.39 Wm^{-2}, 0.30 Wm^{-2}, 0.18 Wm^{-2}, and 0.31 Wm^{-2}, respectively. The corresponding values in TP were 0.42 Wm^{-2}, 0.05 Wm^{-2}, −0.14 Wm^{-2}, −0.06 Wm^{-2}, and −0.02 Wm^{-2} from May to September. However, we note that these values represent broad spatial and temporal averages and should be interpreted as approximate potential differences in surface net radiation rather than absolute radiative forcing factors.

4. Discussion

4.1. Attribution of albedo changes to vegetation from different perspectives of space, time and spectral bands

This study examined the complex correlations between land surface albedo and EVI2 in grasslands of China for the different broadbands of albedo (SW, VIS, and NIR), each month of the growing season (from May to September), and different regions (IM and TP). Generally, the SW albedo decreased where EVI2 increased (Fig. 2a and b). The NIR albedo was either positively or negatively correlated with EVI2 in different regions (IM and TP), while the VIS albedo was negatively correlated with EVI2 in most of the grasslands (Fig. 3b and c). The number of pixels that had a significant correlation between EVI2 and VIS albedo was almost two times than that of EVI2 and NIR albedo (Fig. 3d), which indicated that the VIS albedo was more susceptible to changes in vegetation than the NIR albedo. This result is consistent with the previous research on forests. For example, Lukeš et al. (2016) found that the NIR albedo showed a weaker negative correlation with forest density than that for the VIS albedo in Finland. The possible reason is that vegetation absorbs more solar radiation in the VIS waveband, while reflect and transmit most of the radiation in the NIR waveband, and the reflection and transmit could be more susceptible to canopy structure and soil albedo other than greenness (Kala et al., 2014).

In terms of different periods, previous studies found that in TP the decreasing annual albedo primarily resulted from increasing grassland greenness in the growing season (Tian et al., 2017). In this study we found more details about monthly variation in the relationships between albedo and EVI2 during the growing season. Specifically, the correlations between the NIR albedo and EVI2 changed from being negative in May (early growing season) to positive in August in most of the grasslands in TP and northeast IM (Fig. 4b1-b5). The VIS albedo was negatively correlated with EVI2 in most of the grasslands from May to

September (Fig. 4c1-c5). The changes in SW, NIR, and VIS albedos due to EVI2 varied from May to September, but EVI2 was consistently negatively correlated with albedo in May (Fig. 6). Meanwhile, the coefficients of determination in Fig. 6 decreased mostly from May to September. The likely reason is that the relationship between EVI2 and albedo was affected by different amounts of litter and dead biomass coverage which resulted in different ratios of green-to-dead biomass during the growing season. Litter and dead biomass have different spectral characteristics from green biomass and soil which makes the relationship between greenness and albedo more complex, and the canopy scale's albedo of grassland is affected by soil, leaf, stem, and dead material under grass (Gao et al., 2005; Liu et al., 2017; Wang and Davidson, 2007).

As for regional differences, the change in albedo varied in IM and TP (Fig. 6). In IM, albedo was negatively correlated with EVI2, which was consistent with previous studies (Li et al., 2016; Planque et al., 2017). For instance, Planque et al. (2017) showed the negative correlation between albedo and NDVI at a French forest site. Li et al. (2016) showed that there was a negative correlation between albedo and NDVI in all researched catchments in the Loess Plateau. The regression slopes of NDVI and albedo in Loess Plateau were steeper than that in TP and were similar with our results (Li et al., 2016; Shen et al., 2015). In the IM region, where soil is brighter resulting from sandy surfaces and poorly organic, the soil albedo differs greatly from the vegetation albedo. When the vegetation turns green, the contribution of the soil albedo to the overall albedo is decreasing, which leads to the strong negative correlation between vegetation greenness and albedo, and the proportion of pixels with significant correlation is relatively high. Especially, due to relatively low LAI and canopy height (Huang et al., 2017), the change of fractional area covered by vegetation and soil plays a more important role in NIR albedo than another factor of canopy development resulting in increased scattering. Unlike the IM region, we found that the negative correlation between EVI2 and SW albedo was only significant in May and June in TP, while there were no significant negative correlations in other months (Fig. 6). The possible reasons are that soil moisture is relatively high in middle of growing season (Zeng et al., 2015) which darken the soil color, and soil is abundantly organic leading to the lower soil reflectance in VIS spectral band, and thus the difference in the reflectance of soil and vegetation is reduced and smaller than that in IM. Another reason is that the NIR albedo increases with canopy development due to increased multiple scattering within the canopy in TP with relatively high LAI (Gates, 1965) and canopy height (Huang et al., 2017). Hammerle et al. (2007) also reported that albedo increased with green area index (GAI) in a temperate grassland in Austria. This phenomenon is similar with the overall albedo increase in the shrub-covered areas of the sub-Arctic due to increasing optical scattering in the NIR spectral region (Williamson et al., 2016). Albedo may not be constantly negatively correlated with vegetation greening, which depended on geographic and seasonal differences (Blok et al., 2011; Lukeš et al., 2014). Notably, the relationship between albedo and EVI2 showed similar pattern in northeastern IM and TP. This phenomenon is due to that these two regions own more moist soil and higher LAI (canopy density) than the southwestern IM region.

Our analysis indicated that the different relationships between albedo and EVI2 in IM and TP regions may be due to the differences in soil albedos which depends on the soil texture, soil organic deposition and soil moisture (Carrer et al., 2014; Song, 1999). Our observed regional differences matched the regional differences found in bare soil albedos using the Kalman Filter method and MODIS data (Carrer et al., 2014). The average soil albedo of the IM region was approximately 0.20–0.30 and the soil albedo of TP was approximately 0.15–0.20. (Carrer et al., 2014). The bigger difference of albedo between vegetation and soil results in higher sensitivity of albedo to EVI2 because changes in canopy cover rapidly change the contribution of vegetation and bare soil albedo to the overall surface albedo (Liu et al., 2017; Sanchez-Mejia et al., 2014), and in some cases the albedo increased as canopy cover increased, which may be attributed to relatively low soil reflectance (Hammerle et al., 2007). Land surface albedo is vital for land surface models which calculate albedo as a function of vegetation and soil albedos in the snow-free period. Thus, it is important to estimate the albedo of bare soil accurately and consider the interaction between vegetation and soil more reasonably (Kala et al., 2014; Rechid et al., 2009; Wang et al., 2016; Yin et al., 2016).

Phenology and the different rates of change in NDVI have important influences on albedo (Song, 1999). Our results showed that the increase of absorbed shortwave radiation caused by the increase of EVI2 by 0.01 was largest in May (early growing season, Fig. 7). One reason is that the regression slope of EVI2 and SW albedo was steepest in May (Fig. 6), and another reason is that the value of surface downward shortwave was highest in May (Yang et al., 2010a). The regression slope in May was highest during growing reason as the variation in vegetation (conversion from low greenness to high greenness) will quickly change the contribution of soil reflectance to surface albedo (Liu et al., 2017). This is consistent with the more significant correlation between the albedo and NDVI variation (quick conversion from low greenness to high greenness) in the sparsely vegetated zone (Tian et al., 2014).

Previous studies have reported the increased rates of NDVI in each season are different (Piao et al., 2011; Sun and Qin, 2016). Spring is an important season for vegetation greening, because the rate of increase in NDVI in spring was larger than in other seasons for TP (Zhang et al., 2013b). Moreover, the phenology of vegetation has been affected by climate change because warming has lengthened the growing season in most of the TP (Sun et al., 2015; Wang et al., 2017a; Zhang et al., 2013a). Loranty et al. (2011) suggested that the albedo correlated with vegetation changes in rapid spring transition has an important impact on surface energy budgets. Therefore, the phenology and vegetation greenness dynamics due to climate change will have incremental potential impacts on albedo and surface energy budgets.

4.2. Uncertainties and implications

The effects of EVI2 on albedo may have two natural processes in the TP region, especially for May: vegetation greening and length of the growing season, which could be affected by snow cover. Previous studies indicated that snow cover considerably affects surface albedo (Li et al., 2018). Snow cover may distort the relationship between albedo and EVI2, although the snow cover in the TP showed no widespread decline (Wang et al., 2017b). Particularly, the snow cover fraction in TP is larger in May and October than the other months of growing season (Pu et al., 2007). Therefore, we construct maps of the dominant driver (snow cover or EVI2) influencing the SW, NIR and VIS albedos in every month of the growing season, respectively (Fig. 8). Snow cover is identified as the foremost important driver of the SW, NIR, and VIS albedos in TP in May (Fig. 8a). For example, for the SW albedo, 61.2% of the studied region in TP is dominated by snow cover in May, in contrast, only about 20.5%, 9.7%, 11.5% and 34.1% of the total pixels was dominated by snow cover in other months. However, the main driver in IM is EVI2, with more than 99% of the pixels being dominated by EVI2 in the whole growing season. The snow cover could depress the value of EVI2 and elevate the value of SW albedo in the TP region. The correlation between SW albedo and EVI2 in this study was likely affected by snow cover in May in TP, and yet rarely affected by snow cover in IM.

In this study, we mainly focused on the relationship between greenness and albedo. However, human-induced land use changes, such as agricultural expansion and grassland restoration, could affect land surface albedo as well (Houspanossian et al., 2017; Loranty et al., 2011; Lukeš et al., 2016; Zhai et al., 2015). Moreover, regional climate change, especially increased temperatures, is affected by radiation/energy fluxes, including absorbed shortwave radiation, evapotranspiration, and other factors (Lee et al., 2011; Peng et al., 2014; Shen

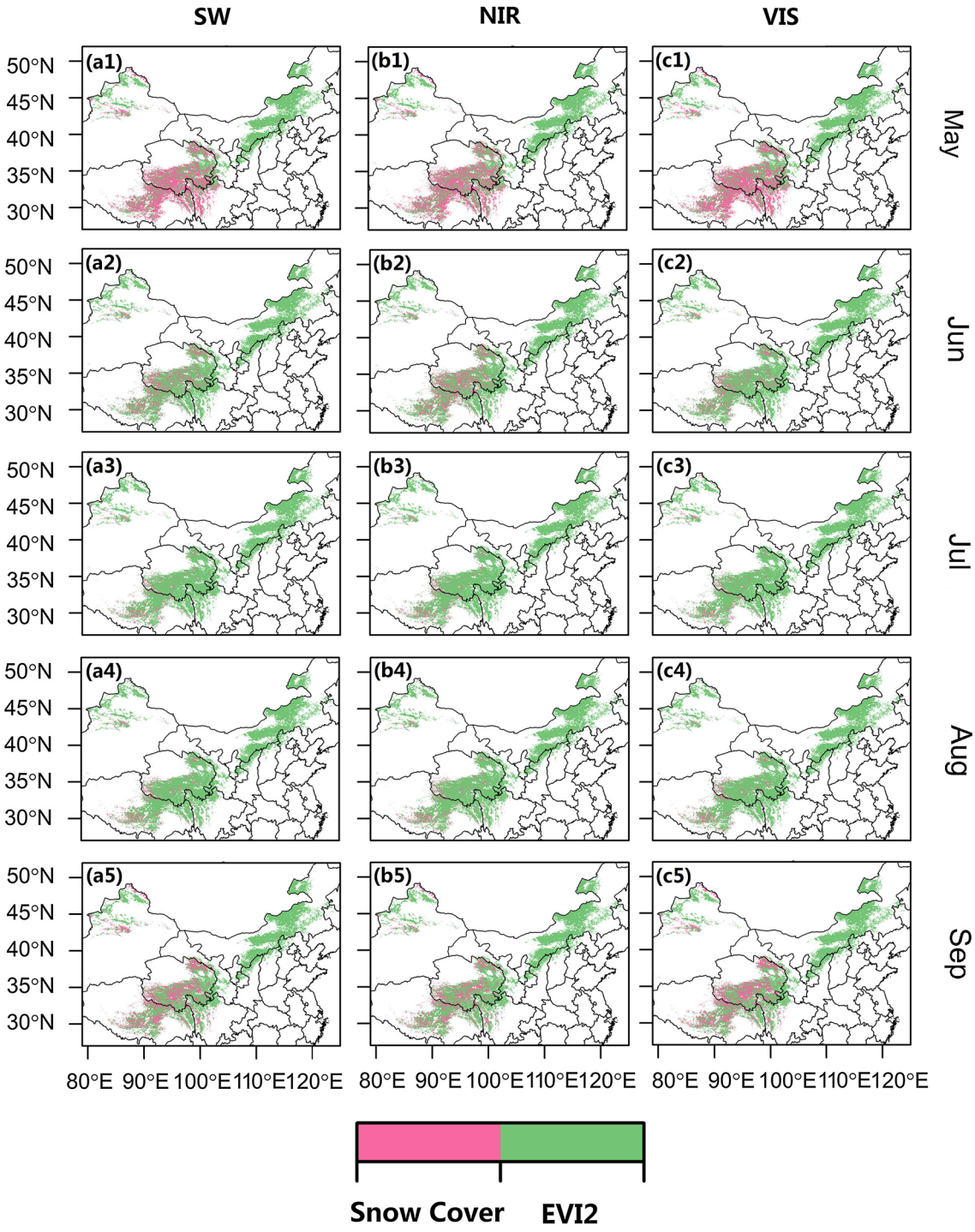

Fig. 8. The dominant factor influencing variations in albedo defined as the driving factor that contributes the most to the increase (or decrease) in albedo in each grid cell.

et al., 2015; Yuan et al., 2017; Zhao et al., 2018). Thus, the relationships between albedo and vegetation dynamics controlled by anthropogenic activities should be investigated in future studies. In addition, effects of phenology change as well as species composition on albedo also need to be explored in the future.

5. Conclusions

In this study, we detected spatial, temporal, and spectral variability in albedo due to greenness changes in the grasslands of China. We found that more than half of grasslands (67.0%) experienced a greening trend with 22.0% significant while 78%, (28.5% significant), 53% (15.6% significant) and 87% (35.3% significant) of grasslands showed decreased trends in the SW, NIR, and VIS albedos, respectively. VIS albedo was more sensitive to vegetation change than NIR albedo. Also, VIS albedo was negatively correlated with EVI2 in all the months of growing season in most of China's grasslands. However, the negative correlation between SW/NIR albedo and EVI2 mainly occurred in the early growing season, but changed to a positive correlation in some regions in TP and the northern part of IM. Through analyzing the spatial

patterns of correlations between EVI2 and albedo, we found two different modes in temperate (IM) and alpine grasslands (TP). Soil moisture induced soil albedo differences could be a potential reason for the different modes of albedo-EVI2 relationships in IM and TP. The greater change in albedo due to grassland greenness in IM indicated that this region had a relatively larger influence on the land surface energy budget and climate. Considering future grassland cover changes due to climate change, these biophysical feedbacks via albedo should be considered. The findings in this study about the spatial, temporal, and spectral variations in albedo responses to grassland greenness changes in China improve our understanding of land-atmosphere interactions and are helpful for improving land surface models.

Acknowledgments

This study is funded by Strategic Priority Research Program (XDA19040301) and Key Research Program of Frontier Sciences (QYZDB-SSW-DQC005) of Chinese Academy of Sciences (CAS), the National Natural Science Foundation of China (41701501, 41501054), and the “Thousand Youth Talents Plan”. We thank Drs. Geli Zhang, Weijun Sun for their valuable comments in the earlier versions of the manuscript. We would also like to acknowledge the valuable comments and suggestions from the editor and four anonymous reviewers in improving this study.

Appendix A. Supplementary material

Supplementary data to this article can be found online at https://doi.org/10.1016/j.isprsjprs.2019.03.020.

References

Betts, R.A., 2000. Offset of the potential carbon sink from boreal forestation by decreases in surface albedo. Nature 408 (6809), 187–190.
Blok, D., Schaepman-Strub, G., Bartholomeus, H., Heijmans, M.M.P.D., Maximov, T.C., Berendse, F., 2011. The response of Arctic vegetation to the summer climate: relation between shrub cover, NDVI, surface albedo and temperature. Environ. Res. Lett. 6 (3) 035502.
Bonan, G.B., 2008. Forests and climate change: forcings, feedbacks, and the climate benefits of forests. Science 320 (5882), 1444–1449.
Brovkin, V., Claussen, M., Driesschaert, E., Fichefet, T., Kicklighter, D., Loutre, M.F., Matthews, H.D., Ramankutty, N., Schaeffer, M., Sokolov, A., 2006. Biogeophysical effects of historical land cover changes simulated by six Earth system models of intermediate complexity. Clim. Dyn. 26 (6), 587–600.
Carrer, D., Meurey, C., Ceamanos, X., Roujean, J.-L., Calvet, J.-C., Liu, S., 2014. Dynamic mapping of snow-free vegetation and bare soil albedos at global 1km scale from 10-year analysis of MODIS satellite products. Remote Sens. Environ. 140, 420–432.
Chen, J., John, R., Shao, C., Fan, Y., Zhang, Y., Amarjargal, A., Brown, D.G., Qi, J., Han, J., Lafortezza, R., Dong, G., 2015. Policy shifts influence the functional changes of the CNH systems on the Mongolian plateau. Environ. Res. Lett. 10 (8) 085003.
Coll, J., Li, X., 2018. Comprehensive accuracy assessment of MODIS daily snow cover products and gap filling methods. ISPRS J. Photogramm. Remote Sens. 144, 435–452.
Coners, H., Babel, W., Willinghöfer, S., Biermann, T., Köhler, L., Seeber, E., Foken, T., Ma, Y., Yang, Y., Miehe, G., Leuschner, C., 2016. Evapotranspiration and water balance of high-elevation grassland on the Tibetan Plateau. J. Hydrol. 533, 557–566.
Didan, K., Barreto, A., 2016. NASA MEaSUREs Vegetation Index and Phenology (VIP) Phenology EVI2 Yearly Global 0.05Deg CMG, distributed by NASA EOSDIS Land Processes DAAC, https://doi.org/10.5067/MEaSUREs/VIP/VIPPHEN_EVI2.004.
Friedl, M.A., Sulla-Menashe, D., Tan, B., Schneider, A., Ramankutty, N., Sibley, A., Huang, X.M., 2010. MODIS collection 5 global land cover: Algorithm refinements and characterization of new datasets. Remote Sens. Environ. 114 (1), 168–182.
Gao, F., Schaaf, C.B., Strahler, A.H., Roesch, A., Lucht, W., Dickinson, R., 2005. MODIS bidirectional reflectance distribution function and albedo climate modeling grid products and the variability of albedo for major global vegetation types. J. Geophys. Res. Atmos. 110 (D1).
Gates, D.M., 1965. Energy, plants, and ecology. Ecology 46 (1–2), 1–13.
Govindasamy, B., Duffy, P.B., Caldeira, K., 2001. Land use changes and northern hemisphere cooling. Geophys. Res. Lett. 28 (2), 291–294.
Grömping, U., 2006. Relative importance for linear regression in R: the package relaimpo. J. Stat. Softw. 17 (1), 1–27.
Hammerle, A., Haslwanter, A., Tappeiner, U., Cernusca, A., Wohlfahrt, G., 2007. Leaf area controls on energy partitioning of a temperate mountain grassland. Biogeosciences 5 (2), 421–431.
He, T., Liang, S., Song, D.-X., 2014. Analysis of global land surface albedo climatology and spatial-temporal variation during 1981–2010 from multiple satellite products. J. Geophys. Res. Atmos. 119 (17), 10281–10298.
Hou, X., Feng, L., Chen, X., Zhang, Y., 2018. Dynamics of the wetland vegetation in large lakes of the Yangtze Plain in response to both fertilizer consumption and climatic changes. ISPRS J. Photogramm. Remote Sens. 141, 148–160.
Houspanossian, J., Giménez, R., Jobbágy, E., Nosetto, M., 2017. Surface albedo raise in the South American Chaco: Combined effects of deforestation and agricultural changes. Agric. For. Meteorol. 232, 118–127.
Huang, H., Liu, C., Wang, X., Biging, G.S., Chen, Y., Yang, J., Gong, P., 2017. Mapping vegetation heights in China using slope correction ICESat data, SRTM, MODIS-derived and climate data. ISPRS J. Photogramm. Remote Sens. 129, 189–199.
Huang, K., Xia, J., Wang, Y., Ahlstrom, A., Chen, J., Cook, R.B., Cui, E., Fang, Y., Fisher, J.B., Huntzinger, D.N., Li, Z., Michalak, A.M., Qiao, Y., Schaefer, K., Schwalm, C., Wang, J., Wei, Y., Xu, X., Yan, L., Bian, C., Luo, Y., 2018. Enhanced peak growth of global vegetation and its key mechanisms. Nat. Ecol. Evol. 2 (12), 1897–1905.
Jiang, Z., Huete, A., Didan, K., Miura, T., 2008. Development of a two-band enhanced vegetation index without a blue band. Remote Sens. Environ. 112 (10), 3833–3845.
Kala, J., Evans, J.P., Pitman, A.J., Schaaf, C.B., Decker, M., Carouge, C., Mocko, D., Sun, Q., 2014. Implementation of a soil albedo scheme in the CABLEv1.4b land surface model and evaluation against MODIS estimates over Australia. Geosci. Model Dev. 7 (5), 2121–2140.
Kang, L., Han, X., Zhang, Z., Sun, O.J., 2007. Grassland ecosystems in China: review of current knowledge and research advancement. Philos. Trans. R. Soc. London, Ser. B 362 (1482), 997–1008.
Kato, S., Loeb, N.G., Rose, F.G., Doelling, D.R., Rutan, D.A., Caldwell, T.E., Yu, L., Weller, R.A., 2013. Surface irradiances consistent with CERES-derived top-of-atmosphere shortwave and longwave irradiances. J. Clim. 26 (9), 2719–2740.
Kim, Y., Kimball, J.S., Zhang, K., Didan, K., Velicogna, I., McDonald, K.C., 2014. Attribution of divergent northern vegetation growth responses to lengthening non-frozen seasons using satellite optical-NIR and microwave remote sensing. Int. J. Remote Sens. 35 (10), 3700–3721.
Kuusinen, N., Stenberg, P., Korhonen, L., Rautiainen, M., Tomppo, E., 2016. Structural factors driving boreal forest albedo in Finland. Remote Sens. Environ. 175, 43–51.
Lee, R., Yu, F., Price, K.P., Ellis, J., Shi, P., 2002. Evaluating vegetation phenological patterns in Inner Mongolia using NDVI time-series analysis. Int. J. Remote Sens. 23 (12), 2505–2512.
Lee, X., Goulden, M.L., Hollinger, D.Y., Barr, A., Black, T.A., Bohrer, G., Bracho, R., Drake, B., Goldstein, A., Gu, L., Katul, G., Kolb, T., Law, B.E., Margolis, H., Meyers, T., Monson, R., Munger, W., Oren, R., Paw, U.K., Richardson, A.D., Schmid, H.P., Staebler, R., Wofsy, S., Zhao, L., 2011. Observed increase in local cooling effect of deforestation at higher latitudes. Nature 479 (7373), 384–387.
Li, Q., Ma, M., Wu, X., Yang, H., 2018. Snow cover and vegetation-induced decrease in global albedo from 2002 to 2016. J. Geophys. Res. Atmos. 123 (1), 124–138.
Li, S., Liang, W., Fu, B., Lu, Y., Fu, S., Wang, S., Su, H., 2016. Vegetation changes in recent large-scale ecological restoration projects and subsequent impact on water resources in China's Loess Plateau. Sci. Total Environ. 569–570, 1032–1039.
Liang, S., Shuey, C.J., Russ, A.L., Fang, H., Chen, M., Walthall, C.L., Daughtry, C.S.T., Hunt, R., 2003. Narrowband to broadband conversions of land surface albedo: II. Validation. Remote Sens. Environ. 84 (1), 25–41.
Liu, D., Li, Y., Wang, T., Peylin, P., MacBean, N., Ciais, P., Jia, G.S., Ma, M.G., Ma, Y.M., Shen, M.G., Zhang, X.Z., Piao, S.L., 2018. Contrasting responses of grassland water and carbon exchanges to climate change between Tibetan Plateau and Inner Mongolia. Agric. For. Meteorol. 249, 163–175.
Liu, F., Chen, Y., Lu, H., Shao, H., 2017. Albedo indicating land degradation around the Badain Jaran Desert for better land resources utilization. Sci. Total Environ. 578, 67–73.
Liu, Q., Wang, L., Qu, Y., Liu, N., Liu, S., Tang, H., Liang, S., 2013. Preliminary evaluation of the long-term GLASS albedo product. Int. J. Digital Earth 6 (sup1), 69–95.
Loarie, S.R., Lobell, D.B., Asner, G.P., Mu, Q., Field, C.B., 2011. Direct impacts on local climate of sugar-cane expansion in Brazil. Nat. Clim. Change 1 (2), 105–109.
Loranty, M.M., Goetz, S.J., Beck, P.S.A., 2011. Tundra vegetation effects on pan-Arctic albedo. Environ. Res. Lett. 6 (2) 024014.
Lukeš, P., Rautiainen, M., Manninen, T., Stenberg, P., Mõttus, M., 2014. Geographical gradients in boreal forest albedo and structure in Finland. Remote Sens. Environ. 152, 526–535.
Lukeš, P., Stenberg, P., Mõttus, M., Manninen, T., Rautiainen, M., 2016. Multidecadal analysis of forest growth and albedo in boreal Finland. Int. J. Appl. Earth Obs. Geoinf. 52, 296–305.
Ma, H., Liang, S., Xiao, Z., Shi, H., 2017. Simultaneous inversion of multiple land surface parameters from MODIS optical–thermal observations. ISPRS J. Photogramm. Remote Sens. 128, 240–254.
Moody, E.G., King, M.D., Schaaf, C.B., Hall, D.K., Platnick, S., 2007. Northern Hemisphere five-year average (2000–2004) spectral albedos of surfaces in the presence of snow: Statistics computed from Terra MODIS land products. Remote Sens. Environ. 111 (2), 337–345.
Peng, S.S., Piao, S., Zeng, Z., Ciais, P., Zhou, L., Li, L.Z., Myneni, R.B., Yin, Y., Zeng, H., 2014. Afforestation in China cools local land surface temperature. PNAS 111 (8), 2915–2919.
Piao, S., Wang, X., Ciais, P., Zhu, B., Wang, T.A.O., Liu, J.I.E., 2011. Changes in satellite-derived vegetation growth trend in temperate and boreal Eurasia from 1982 to 2006. Global Change Biol. 17 (10), 3228–3239.
Planque, C., Carrer, D., Roujean, J.-L., 2017. Analysis of MODIS albedo changes over steady woody covers in France during the period of 2001–2013. Remote Sens. Environ. 191, 13–29.
Pu, Z., Xu, L., Salomonson, V.V., 2007. MODIS/Terra observed seasonal variations of snow cover over the Tibetan Plateau. Geophys. Res. Lett. 34 (6).
Rechid, D., Raddatz, T.J., Jacob, D., 2009. Parameterization of snow-free land surface albedo as a function of vegetation phenology based on MODIS data and applied in

climate modelling. Theor. Appl. Climatol. 95 (3–4), 245–255.
Sanchez-Mejia, Z.M., Papuga, S.A., Swetish, J.B., van Leeuwen, W.J.D., Szutu, D., Hartfield, K., 2014. Quantifying the influence of deep soil moisture on ecosystem albedo: The role of vegetation. Water Resour. Res. 50 (5), 4038–4053.
Shen, M., Piao, S., Jeong, S.J., Zhou, L., Zeng, Z., Ciais, P., Chen, D., Huang, M., Jin, C.S., Li, L.Z., Li, Y., Myneni, R.B., Yang, K., Zhang, G., Zhang, Y., Yao, T., 2015. Evaporative cooling over the Tibetan Plateau induced by vegetation growth. PNAS 112 (30), 9299–9304.
Song, J., 1999. Phenological influences on the albedo of prairie grassland and crop fields. Int. J. Biometeorol. 42 (3), 153–157.
Sun, J., Qin, X., 2016. Precipitation and temperature regulate the seasonal changes of NDVI across the Tibetan Plateau. Environ. Earth Sci. 75 (4).
Sun, W., Song, X., Mu, X., Gao, P., Wang, F., Zhao, G., 2015. Spatiotemporal vegetation cover variations associated with climate change and ecological restoration in the Loess Plateau. Agric. For. Meteorol. 209–210, 87–99.
Tian, L., Chen, J., Zhang, Y., 2017. Growing season carries stronger contributions to albedo dynamics on the Tibetan plateau. PLoS One 12 (9) e0180559.
Tian, L., Zhang, Y., Zhu, J., 2014. Decreased surface albedo driven by denser vegetation on the Tibetan Plateau. Environ. Res. Lett. 9 (10) 104001.
Wang, R., Chen, J.M., Pavlic, G., Arain, A., 2016. Improving winter leaf area index estimation in coniferous forests and its significance in estimating the land surface albedo. ISPRS J. Photogramm. Remote Sens. 119, 32–48.
Wang, S., Davidson, A., 2007. Impact of climate variations on surface albedo of a temperate grassland. Agric. For. Meteorol. 142 (2–4), 133–142.
Wang, S., Zhang, B., Yang, Q., Chen, G., Yang, B., Lu, L., Shen, M., Peng, Y., 2017a. Responses of net primary productivity to phenological dynamics in the Tibetan Plateau. China. Agric. For. Meteorol. 232, 235–246.
Wang, X., Wu, C., Wang, H., Gonsamo, A., Liu, Z., 2017b. No evidence of widespread decline of snow cover on the Tibetan Plateau over 2000–2015. Sci. Rep. 7 (1), 14645.
Williamson, S.N., Barrio, I.C., Hik, D.S., Gamon, J.A., 2016. Phenology and species determine growing-season albedo increase at the altitudinal limit of shrub growth in the sub-Arctic. Glob Chang Biol. 22 (11), 3621–3631.
Yang, K., He, J., Tang, W., Qin, J., Cheng, C.C.K., 2010a. On downward shortwave and longwave radiations over high altitude regions: Observation and modeling in the Tibetan Plateau. Agric. For. Meteorol. 150 (1), 38–46.
Yang, Y., Fang, J., Fay, P.A., Bell, J.E., Ji, C., 2010b. Rain use efficiency across a precipitation gradient on the Tibetan Plateau. Geophys. Res. Lett. 37 (15), n/a-n/a.
Yin, J., Zhan, X., Zheng, Y., Hain, C.R., Ek, M., Wen, J., Fang, L., Liu, J., 2016. Improving Noah land surface model performance using near real time surface albedo and green vegetation fraction. Agric. For. Meteorol. 218–219, 171–183.
You, Q., Fraedrich, K., Ren, G., Pepin, N., Kang, S., 2013. Variability of temperature in the Tibetan Plateau based on homogenized surface stations and reanalysis data. Int. J. Climatol. 33 (6), 1337–1347.
Yuan, X., Wang, W., Cui, J., Meng, F., Kurban, A., De Maeyer, P., 2017. Vegetation changes and land surface feedbacks drive shifts in local temperatures over Central Asia. Sci. Rep. 7 (1), 3287.
Zeng, J., Li, Z., Chen, Q., Bi, H., Qiu, J., Zou, P., 2015. Evaluation of remotely sensed and reanalysis soil moisture products over the Tibetan Plateau using in-situ observations. Remote Sens. Environ. 163, 91–110.
Zeng, Z., Piao, S., Li, L.Z.X., Zhou, L., Ciais, P., Wang, T., Li, Y., Lian, X., Wood, E.F., Friedlingstein, P., Mao, J., Estes, L.D., Myneni, Ranga B., Peng, S., Shi, X., Seneviratne, S.I., Wang, Y., 2017. Climate mitigation from vegetation biophysical feedbacks during the past three decades. Nat. Clim. Change 7 (6), 432–436.
Zhai, J., Liu, R., Liu, J., Huang, L., Qin, Y., 2015. Human-induced landcover changes drive a diminution of land surface Albedo in the Loess Plateau (China). Remote Sens. 7 (3), 2926–2941.
Zhang, G., Zhang, Y., Dong, J., Xiao, X., 2013a. Green-up dates in the Tibetan Plateau have continuously advanced from 1982 to 2011. PNAS 110 (11), 4309–4314.
Zhang, K., Kimball, J.S., Nemani, R.R., Running, S.W., Hong, Y., Gourley, J.J., Yu, Z., 2015. Vegetation greening and climate change promote multidecadal rises of global land evapotranspiration. Sci. Rep. 5, 15956.
Zhang, L., Guo, H., Ji, L., Lei, L., Wang, C., Yan, D., Li, B., Li, J., 2013b. Vegetation greenness trend (2000 to 2009) and the climate controls in the Qinghai-Tibetan Plateau. J. Appl. Remote Sens. 7 (1) 073572.
Zhang, L., Guo, H., Jia, G., Wylie, B., Gilmanov, T., Howard, D., Ji, L., Xiao, J., Li, J., Yuan, W., Zhao, T., Chen, S., Zhou, G., Kato, T., 2014. Net ecosystem productivity of temperate grasslands in northern China: An upscaling study. Agric. For. Meteorol. 184, 71–81.
Zhao, G., Dong, J., Cui, Y., Liu, J., Zhai, J., He, T., Zhou, Y., Xiao, X., 2018. Evapotranspiration-dominated biogeophysical warming effect of urbanization in the Beijing-Tianjin-Hebei region, China. Clim. Dyn.
Zhu, Z., Piao, S., Myneni, R.B., Huang, M., Zeng, Z., Canadell, J.G., Ciais, P., Sitch, S., Friedlingstein, P., Arneth, A., Cao, C., Cheng, L., Kato, E., Koven, C., Li, Y., Lian, X., Liu, Y., Liu, R., Mao, J., Pan, Y., Peng, S., Peñuelas, J., Poulter, B., Pugh, T.A.M., Stocker, B.D., Viovy, N., Wang, X., Wang, Y., Xiao, Z., Yang, H., Zaehle, S., Zeng, N., 2016. Greening of the Earth and its drivers. Nat. Clim. Change 6 (8), 791–795.